Observation of a fast ozone loss in the marginal ice zone of the Arctic Ocean

Hans-Werner Jacobi,[1] Lars Kaleschke,[2,3] Andreas Richter,[2] Alexei Rozanov,[2] and John P. Burrows[2]

[1] In both polar regions tropospheric ozone regularly decreases during springtime to negligible concentrations in the atmospheric boundary layer. Here we report the observation of a dramatic ozone depletion event in the atmospheric boundary layer in the vicinity of new ice fields in the marginal ice zone (MIZ) of the Arctic Ocean monitored by instrumentation on board the icebreaker RV *Polarstern*. The ozone mixing ratio decreased from approximately 40 to below 1 ppbV in less than 7 hours. The analyses of backward trajectories and the synoptic conditions indicate that the observed decrease was not caused by the transport of ozone-free air, but that the ozone depletion occurred locally. Accordingly, bromine oxide, which is formed during the photochemical destruction of ozone in the presence of reactive bromine compounds, was significantly enhanced: Bromine oxide concentrations of approximately $1.8 \cdot 10^9$ molecules cm^{-3} are retrieved around the same location from SCIAMACHY satellite observations assuming a uniform vertical distribution within the boundary layer. The release of bromine in the MIZ where the new ice formation took place appears to be the most likely explanation for the activation of reactive bromine compounds and subsequent depletion of ozone. Since the conditions were favorable for the formation of frost flowers, we suggest that these are the most likely sources of the reactive bromine. However, contributions of heterogeneous reactions on other surfaces like the highly saline brine on the new ice, aerosols generated from frost flowers, and sea salt aerosols deposited on the snowpack on top of the sea ice cannot be ruled out.

Citation: Jacobi, H.-W., L. Kaleschke, A. Richter, A. Rozanov, and J. P. Burrows (2006), Observation of a fast ozone loss in the marginal ice zone of the Arctic Ocean, *J. Geophys. Res.*, *111*, D15309, doi:10.1029/2005JD006715.

1. Introduction

[2] The depletion of ozone (O_3) in the atmospheric boundary layer at high latitudes is a remarkable phenomenon, which was first reported almost 20 years ago [*Bottenheim et al.*, 1986; *Oltmans and Komhyr*, 1986; *Barrie et al.*, 1988]. Such O_3 depletion events (ODEs) having mixing ratios below 10 ppbV (parts per billion by volume) occur regularly in the atmospheric boundary layer at high latitude during springtime in the Arctic [e.g., *Tarasick and Bottenheim*, 2002] and the Antarctic [e.g., *Wessel et al.*, 1998]. Over the Arctic Ocean ODEs are widespread phenomena [*Ridley et al.*, 2003] covering up to 20% of the area of the northern high latitudes [*Zeng et al.*, 2003]. ODEs have been linked with high levels of filterable bromine [*Barrie et al.*, 1988], the presence of BrO clouds [*Wagner and Platt*, 1998], and the loss of gaseous elemental mercury from the atmosphere [*Schroeder et al.*, 1998].

[3] The O_3 destruction is driven and accompanied by high levels of halogen oxides. It proceeds via several catalytic reaction cycles. *Platt and Hönninger* [2003] described different catalytic reaction cycles involving halogen oxides, which can cause an efficient destruction of tropospheric O_3.

Catalytic cycle 1:

(R1) $\qquad 2(X + O_3 \rightarrow XO + O_2)$

(R2) $\qquad XO + XO \rightarrow 2\ X + O_2$

(R3) $\qquad XO + XO \rightarrow X_2 + O_2$

(R4) $\qquad X_2 + h\nu \rightarrow 2\ X$

$\qquad$ Net: $\quad 2\ O_3 \rightarrow 3\ O_2$

Catalytic cycle 2:

$\qquad X + O_3 \rightarrow XO + O_2$
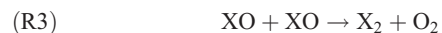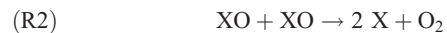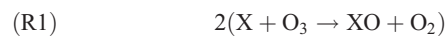
(R5) $\qquad OH + O_3 \rightarrow HO_2 + O_2$
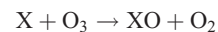
[1]Alfred Wegener Institute for Polar and Marine Research, Bremerhaven, Germany.

[2]Institute of Environmental Physics, University of Bremen, Bremen, Germany.

[3]Now at Institute of Oceanography, Center for Marine and Atmospheric Research, University of Hamburg, Hamburg, Germany.
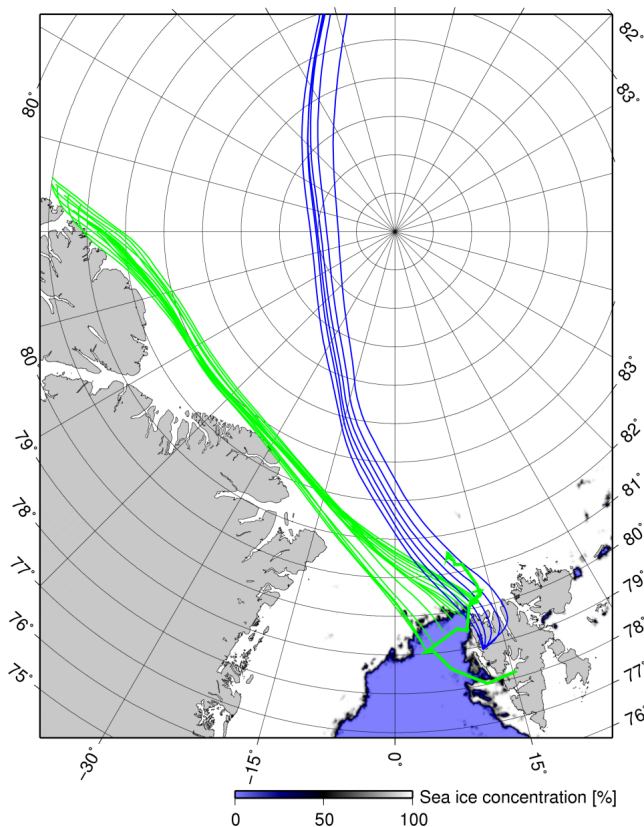
Figure 1. Sea ice concentration derived from AMSR-E 89 GHz data for 31 March. The thick green line indicates a part (29–31 March) of the cruise track of RV *Polarstern* west and northwest of Spitsbergen (ARK XIX/1). Green and blue lines indicate 72-hour backward trajectories for RV *Polarstern* and Zeppelin Station, Ny-Ålesund. Trajectories are shown for the period between 1200 UTC on 30 March and 1800 UTC on 31 March. Starting points of the trajectories are either the actual ship's positions or the Zeppelin station.

(R6) $\qquad HO_2 + XO \rightarrow HOX + O_2$

(R7) $\qquad HOX + h\nu \rightarrow OH + X$

$\qquad$ Net : $\quad 2\,O_3 + h\nu \rightarrow 3\,O_2$

Catalytic cycle 3:

(R8) $\qquad XY + h\nu \rightarrow X + Y$

$\qquad\qquad X + O_3 \rightarrow XO + O_2$

(R9) $\qquad Y + O_3 \rightarrow YO + O_2$

(R10) $\qquad XO + YO \rightarrow X + YO_2$

(R11) $\qquad YO_2 + M \rightarrow Y + O_2 + M$

$\qquad$ Net : $\quad 2\,O_3 + h\nu \rightarrow 3\,O_2$
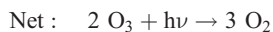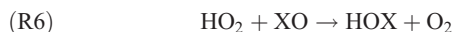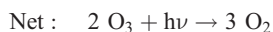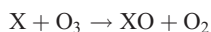
[4] In these reactions X and Y represent Cl, Br, or I, X_2 represents Cl_2, Br_2, or I_2, HOX represents HOCl or HOBr, and XY represents BrCl, BrI, or ClI. As large amounts of bromine oxide (BrO) have been observed in ODEs and some evidence for a small activation of Cl exists, our current understanding is that X, X_2, HOX and XY in an ODE are primarily Br, Br_2, HOBr, and BrCl, respectively.

[5] At present, the source of the reactive halogens remains a matter of scientific debate. *Vogt et al.* [1996] proposed an autocatalytic production of photochemically active bromine including the heterogeneous production of molecular bromine (Br_2) on sea salt aerosols. The reactive bromine compounds (Br_2, BrCl) are released to the gas phase and photolyzed forming Br atoms. Interestingly, the gas phase reaction of BrO with HO_2 produces HOBr, which if absorbed into aerosols participates in the heterogeneous oxidation of bromide (Br^-), making the overall process autocatalytic. A similar cycle with reduced efficiency is feasible for ClO because of the significantly smaller photolysis frequency of HOCl compared to HOBr [*Sander et al.*, 2003] and the higher reactivity of Cl toward organics. At present it is not clear whether iodine and IO reactions are playing a significant role in ODEs.

[6] Assuming that the Br chemistry is dominating the ODE, then the chain length or effectiveness of the reaction cycles above depends on the photolysis frequencies of the bromine reservoirs and therefore on the actinic flux of radiation. The autocatalytic nature of the chain of reactions, coupled with the increase of the actinic radiation, implies a rapid growth of reactive bromine compounds after polar sunrise. This has been labeled the "bromine explosion" [e.g., *Wennberg*, 1999; *Platt and Hönninger*, 2003]. Since it appears unlikely that atmospheric aerosol can release sufficient bromine to explain this phenomenon [e.g., *Impey et al.*, 1997; *Lehrer et al.*, 2004], distinct surfaces with specific properties are more likely sources.

[7] Although ODEs are regularly observed at several Arctic stations [*Tarasick and Bottenheim*, 2002], the origin as well as the spatial and temporal extent of Arctic ODEs are not well characterized nor understood. The objective of this study was to identify the conditions necessary for the development of an ODE. Since previous measurements indicate that the Arctic Ocean is the origin of the ODEs, we used the extraordinary opportunity to perform measurements of O_3 on board an icebreaker, which operated in spring in the still ice-covered Arctic Ocean.

2. Methods

[8] Surface O_3 mixing ratios were measured continuously on board the icebreaker RV *Polarstern* during a cruise in the region west and northwest of the Spitsbergen archipelago (Expedition ARK XIX/1). The cruise track started at Bremerhaven, Germany (54°N) on 28 February 2003 and ended in Longyearbyen, Svalbard (78.2°N, 15.6°E) on 24 April 2003. The ship visited the port of Longyearbyen on 29 March and entered the Fram Strait late on the evening of the same day (Figure 1). O_3 was measured between 16 March and 23 April using a commercial detector ($O_3$41M, Ansyco GmbH, Karlsruhe, Germany), which is based on UV photometric detection at 254 nm. The

unheated inlet line consisted of approximately 5 m of 0.8 cm ID perfluoroalkoxy tubing and was mounted on the compass deck rail on the portside approximately 25 m above sea level. The concentrations were internally averaged and stored as 10-min averages resulting in a limit of detection of 1 ppbV.

[9] Standard meteorological data are routinely collected aboard the RV *Polarstern*. Information about the different sensors and their installation on board can be found at http://www.awi-bremerhaven.de/MET/Polarstern/poldatinfo.html. Retrieval of data from the data archive POLDAT is possible starting from http://www.awi-bremerhaven.de/MET/Polarstern/poldatquery.html. In addition, standard radiosondes were regularly launched from the helicopter deck of RV *Polarstern*.

[10] Further O_3 measurements in Spitsbergen are performed year-round at the Zeppelin mountain station (78°54′N, 11°53′E, 474 m above sea level) located on a mountain ridge south of the small research village at Ny-Ålesund (Figure 1). Ozone is monitored at the station by a commercial UV absorption instrument (API 400A # 612, Teledyne, San Diego, CA) with a lower detection limit of 0.6 ppbV. Zero and span checks are performed automatically every second week and a manual calibration is done once a year using a TEI 49 CPS #60955-329 as a reference. The air intake is through a 4.5 m FEP tube with an outer diameter of 0.635 cm and an inner diameter of 0.475 cm. The monitoring is part of the national, Norwegian monitoring program, EMEP (European Monitoring and Evaluation Programme) and GAW (Global Atmospheric Watch). A climatology of the low ozone episodes observed at the Zeppelin station was given by *Solberg et al.* [1996].

[11] Backward trajectories were calculated with the Hybrid Single-Particle Lagrangian Integrated Trajectory (HYSPLIT) Model (R. R. Draxler and G. D. Rolph, NOAA Air Resources Laboratory, Silver Spring, Maryland, model access via http://www.arl.noaa.gov/ready/hysplit4.html, 2003). The model was driven by Final Run reanalysis wind fields (FNL). The trajectories for the RV *Polarstern* cruise were initiated at the actual ship's positions with the starting height at the level of the O_3 measurements (25 m above the ground level). The trajectories for the Zeppelin station were initiated with the station position at an elevation of 475 m.

[12] BrO is one of the reactive halogen compounds, which are generated during the catalytic destruction of O_3. Clouds of elevated BrO can be identified using UV/visible remote sensing techniques from space and have been retrieved from measurements by the Global Ozone Monitoring Experiment (GOME) in both hemispheres [*Wagner and Platt*, 1998; *Richter et al.*, 1998]. In this study data from SCIAMACHY (SCanning Imaging Absorption spectroMeter for Atmospheric CHartographY) [*Bovensmann et al.*, 1999] are used, which has a somewhat improved spatial resolution as compared to GOME (240 km × 30 km compared to 320 km × 40 km for BrO in the region of interest). As the nadir measurements are sensitive to both stratospheric and tropospheric BrO, the stratospheric component must be accounted for before retrieval of the tropospheric amount. In this analysis the stratospheric BrO column over the region around Spitsbergen was determined by integrating the stratospheric BrO profiles

deduced from SCIAMACHY limb measurements [*Rozanov et al.*, 2005] and averaging the results. On the basis of these data, the stratospheric column was approximated with $4 \cdot 10^{13}$ molecules cm^{-2} and subtracted from the total column observed in nadir. The resulting tropospheric slant columns were then converted to vertical columns assuming that BrO is well mixed in a 400 m thick boundary layer at a surface reflectivity of 90%. As both the stratospheric correction and the air mass factor have a large uncertainty, and a BrO background present in the free troposphere could also contribute to the signal, the error of the tropospheric columns is estimated to be of the order of 30%.

[13] The sea ice conditions surrounding the operational area of the vessel was analyzed using remote sensing data. Sea ice concentrations (Figure 1) were derived from 89 GHz AMSR-E data [*Kaleschke et al.*, 2001; G. Spreen et al., Sea ice remote sensing using AMSR-E 89 GHz channels, submitted to *Journal of Geophysical Research*, 2006]. In addition, a MODIS image for 31 March (1125 UTC) was used to investigate new ice formation in the marginal ice zone (MIZ) (Figure 2). Nilas is a type of new ice that forms in quite conditions. This thin elastic crust has a smooth surface and is up to 10 cm in thickness. Light nilas is more than 5 cm in thickness and commonly covered with frost flowers. It exhibits the highest emissivity at 89 GHz ($\varepsilon_v = 0.955$, $\varepsilon_h = 0.925$) as compared with other ice types [*Eppler et al.*, 1992]. Therefore light nilas can be detected with a simple threshold method using passive microwave data. The AMSR-E sensor measures the brightness temperature T_B with a spatial resolution of about 5 km, which is sufficient to detect larger leads. Here, we used a threshold of T_B(V-pol) > 230 K to detect the areas of light nilas.

3. Results and Discussion

[14] Figure 3 shows the O_3 measurements performed between 29 March and 6 April, when the ship traveled from the Isfjord through the Fram Strait to the Arctic Ocean. This part of the O_3 time series covers a period of more than 5 days, during which the O_3 concentrations almost exclusively remained close to or below the detection limit of 1 ppbV. The situation before and during the beginning of the ODE when the O_3 concentrations dropped from 39.7 to below 1 ppbV within less than 7 hours (31 March; 1130 until 1740 UTC) is analyzed in order to identify the specific conditions necessary for the O_3 depletion.

[15] The analysis of ODEs at Arctic stations is complicated by the transport of air masses with low O_3 concentrations to the stations across the Arctic Ocean [*Wessel et al.*, 1998; *Tarasick and Bottenheim*, 2002; *Bottenheim et al.*, 2002]. Only some events have been ascribed to local chemical processes [*Hopper et al.*, 1998; *Boudries and Bottenheim*, 2000]. For the ODE observed on 31 March, the origin of the O_3 decrease was investigated. The possibilities of the transport of O_3-poor air to the measurement location, of the transit of the ship into a region with low O_3 concentrations, and of the local chemical O_3 destruction taking place close to the ship's position were considered.

3.1. Long-Range Transport

[16] Long-range transport of air masses did not show any significant change during the period from 29 March to
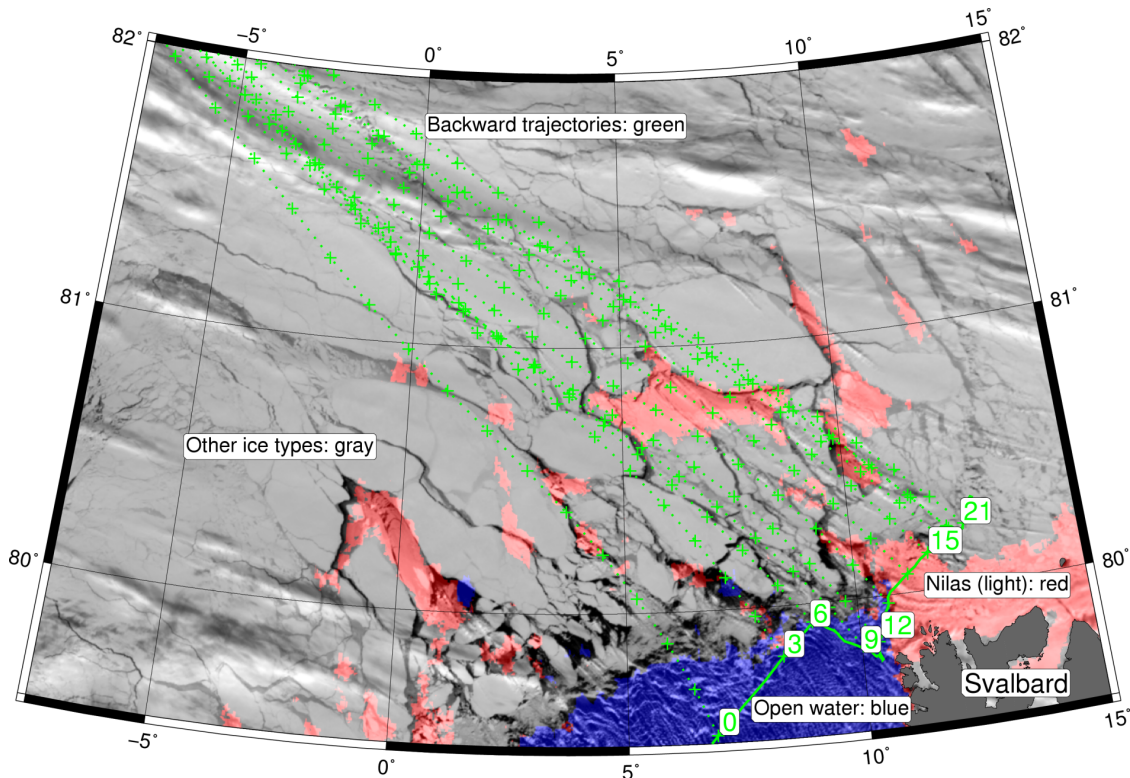
Figure 2. MODIS image (λ = 645 nm, 250 m resolution) for 31 March (1125 UTC) of the region northwest of Svalbard. The thick green line indicates a part of the cruise track of RV *Polarstern* and the corresponding hour of the day. Starting points of atmospheric back trajectories (dotted green line) are the actual ship's position. Crosses mark time steps of 1 hour along the trajectories. Open water (ice concentration <5%) is indicated in blue. Areas covered with light nilas (see text) are indicated in red.

1 April. The synoptic situation was dominated by a stationary high above northern Greenland. This high resulted in a constant meridional flow of air along the northern coast of Greenland into the Fram Strait and to the northwestern tip of Spitsbergen. 72-hour backward air parcel trajectories for the period from 29 March (0000 UTC) to 1 April (2300 UTC) were analyzed. They indicate a stable circulation pattern for the period before, during, and after the O_3 decrease. The trajectories followed similar pathways during the entire period investigated. Selected trajectories covering the period from 30 March (1200 UTC) to 31 March (1800 UTC) are shown as examples in the Figures 1 and 2. Accordingly, the meteorological parameters wind speed, relative humidity, radiation, and air pressure changed only gradually in agreement with the stable mesoscale meteorological conditions (Figure 4). Therefore it appears unlikely that the observed
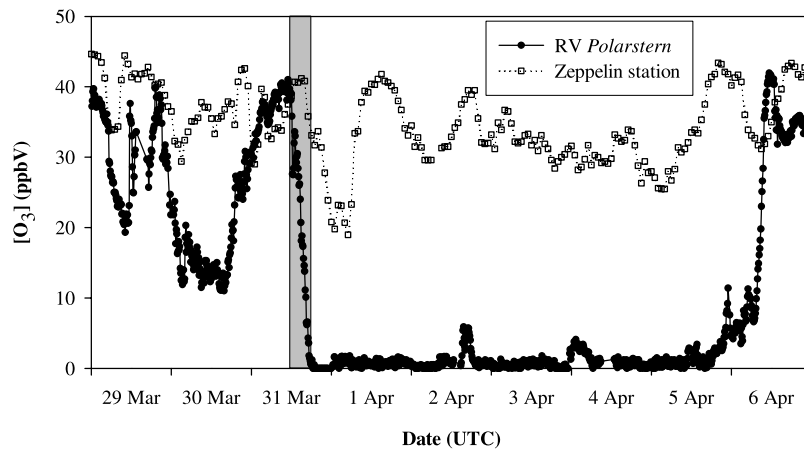
Figure 3. Time series of O_3 concentrations measured on board RV *Polarstern* (10-min averages) and at Zeppelin station (1-hour averages) at Ny-Alesund, Spitsbergen. The shaded area indicates the period when O_3 decreased from 39.7 ppbV (31 March, 1130 UTC) to less than 1 ppbV (31 March, 1740 UTC). Ticks mark midnight of each day.

O_3 decay is due to the change in the long-range transport of different air masses having either normal or low O_3 concentrations.

3.2. Spatial Versus Temporal O_3 Gradient

[17] As the ship was moving during the O_3 decrease, it is possible that the ODE developed earlier and the decreasing O_3 was caused by the transit from a region with normal O_3
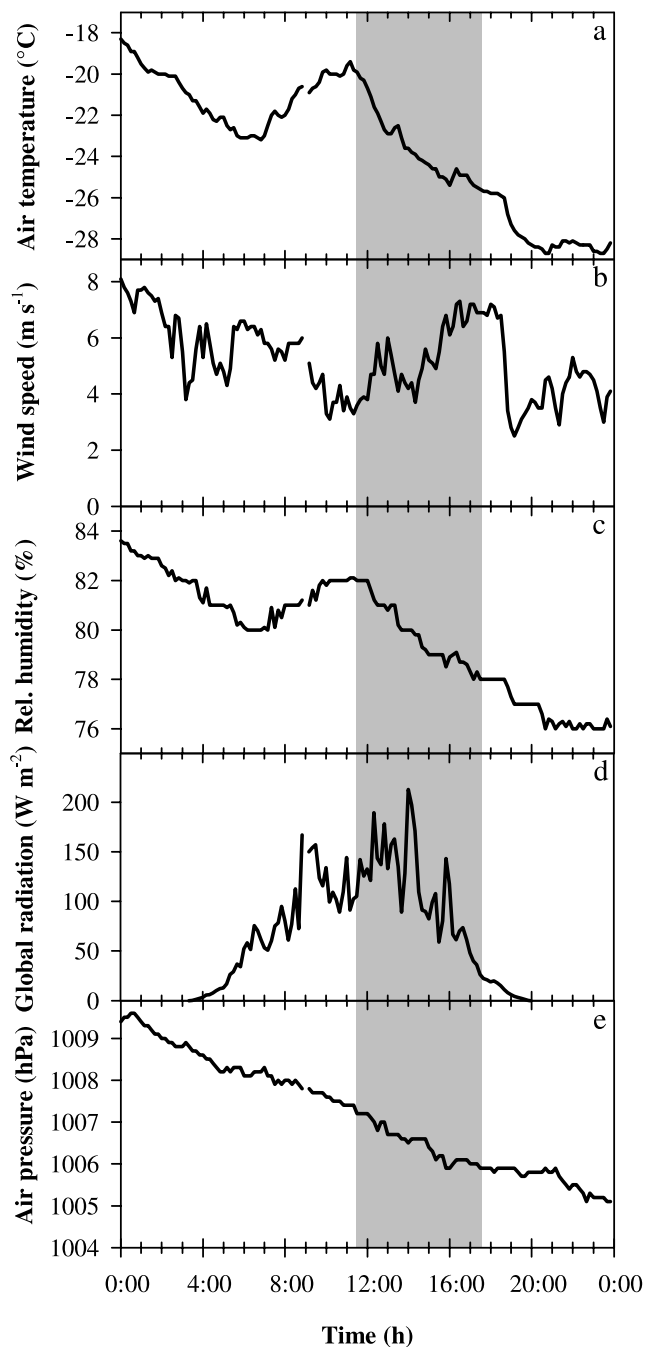
Figure 4. Ten-minute averages of meteorological parameters measured on board RV *Polarstern* on 31 March: (a) air temperature, (b) wind speed, (c) relative humidity, (d) global radiation, and (e) air pressure. The shaded area indicates the period between 1140 and 1730 UTC, when the rapid O_3 depletion occurred.
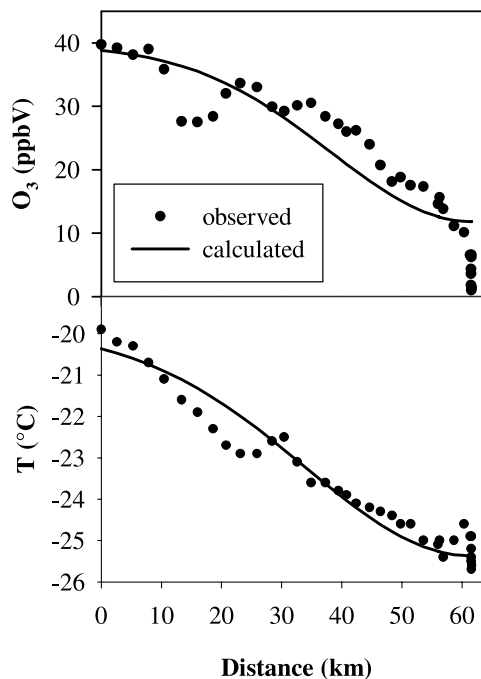
Figure 5. (top) O_3 concentration and (bottom) air temperature as a function of the traveled distance to the ship's location at 1130 UTC on 31 March (79.7629°N, 10.4216°E). The dots represent the measured values. The line shows the calculated transition described by a Gaussian curve according to atmospheric dispersion theory (see auxiliary material).

into the center of the ODE where O_3 was destroyed earlier. However, the distance covered by the ship during the O_3 decrease was less than 62 km. The decrease from more than 15 to 1 ppbV occurred within a distance of 5 km, and the final decrease from more than 10 to 1 ppbV occurred while the ship traveled a distance of 1.3 km (Figure 5). This final O_3 drop while RV *Polarstern* remained almost immobile clearly indicates that the observed O_3 decrease was a temporal, not a spatial decline in the O_3 concentration.

[18] In contrast, the air temperature measured during the same period demonstrates that regarding the meteorological conditions the ship covered a transition between two distinct regions. Figure 5 shows a plot of the observed air temperatures along the transit. In this case, a drop from −19.9°C to approximately −25°C was found. Such a profile can be analyzed using empirical atmospheric dispersion theory (see auxiliary material[1]). The calculated profiles for the air temperature and the O_3 concentration are also shown in Figure 5. These results suggest that the ship covered a transition between two regions with distinct different air temperatures entering an area with significantly lower values. The horizontal temperature profile between these two regions agrees well with the profile expected from atmospheric dispersion theory. Obviously, this is not the case for the observed horizontal O_3 concentration profile although low air temperatures as those found in the entered region are thought to be favorable for the occurrence of ODEs. The shape of the O_3 profile is distinctly different from the expected profile sug-
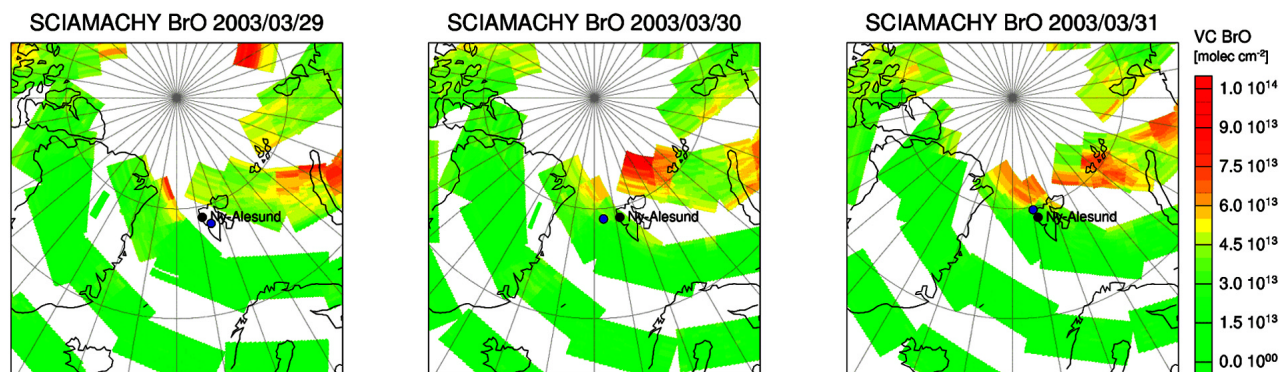
Figure 6. Tropospheric BrO columns as measured by SCIAMACHY. The graphs show daily composite maps, which at high latitudes are the average of up to three measurements. A constant stratospheric BrO column of $4 \cdot 10^{13}$ molecules cm^{-2} was assumed similar to the stratospheric profile measured in limb. Tropospheric columns were derived assuming a well-mixed boundary layer of 400 m and a surface reflectivity of 0.9, which is only appropriate over the ice-covered regions. The gaps result from the alternate limb and nadir scanning of SCIAMACHY. The blue dot indicates the ship position at the time of satellite overpass. However, as the measurements are taken sequentially, the data shown spread over a period of 24 hours.

gesting that the measured O_3 drop is not a spatial feature, but rather developed in time during the observations.

3.3. Bromine Oxide Concentrations

[19] Since the concentration of the BrO radical reaches high levels during the catalytic destruction of O_3 [e.g., *Tuckermann et al.*, 1997], observations of elevated BrO concentrations can support our conclusion. In Figure 6, daily tropospheric BrO columns from SCIAMACHY are shown between 29 and 31 March. A comparison with the map in Figure 2 reveals that BrO was enhanced on 31 March in the same area where the ODE was observed. In contrast, no indication for large BrO enhancements was found in this area on the previous days in the area probed by SCIAMACHY. On 29 March an area with enhanced BrO columns was also detected not far from the northeastern edge of Greenland. Air masses from this area were transported to the operational area of the icebreaker indicated by forward trajectories. However, the trajectories also demonstrate that these air masses were already sampled 24 hours later. In fact, the O_3 time series (Figure 3) exhibits concentrations below 20 ppbV for longer periods on 30 March, which in this case can obviously be attributed to the transport of air with reduced O_3 concentrations to the sampling site.

[20] Measurements of the BrO distribution in the troposphere inferred from multiple angle DOAS measurements at Alert in the Hudson Bay indicate that during the ODE the tropospheric BrO is mainly located in the boundary layer [*Hönninger and Platt*, 2002]. The height of the boundary layer was determined using data from regularly launched radiosondes. Profiles of the potential temperatures measured on 31 March and 1 April are shown in Figure 7. The profile on the morning of 31 March was measured in the open water area not far from the northwestern tip of Spitsbergen. It indicates neutral conditions in the boundary layer up to a height of approximately 380 m. On top of the boundary layer a strong inversion was observed. The profiles measured later in the evening of 31 March and in the morning of 1 April are

representative for the conditions in the MIZ. Here temperatures in the boundary layer are several degrees lower, while temperatures at the height of 1000 m are similar above the open water and in the MIZ. In the MIZ the boundary layer was characterized by either neutral or stable conditions. The temperature inversions on top of the boundary layer were even stronger than in the open water area. The boundary layer heights varied between 220 and 380 m.
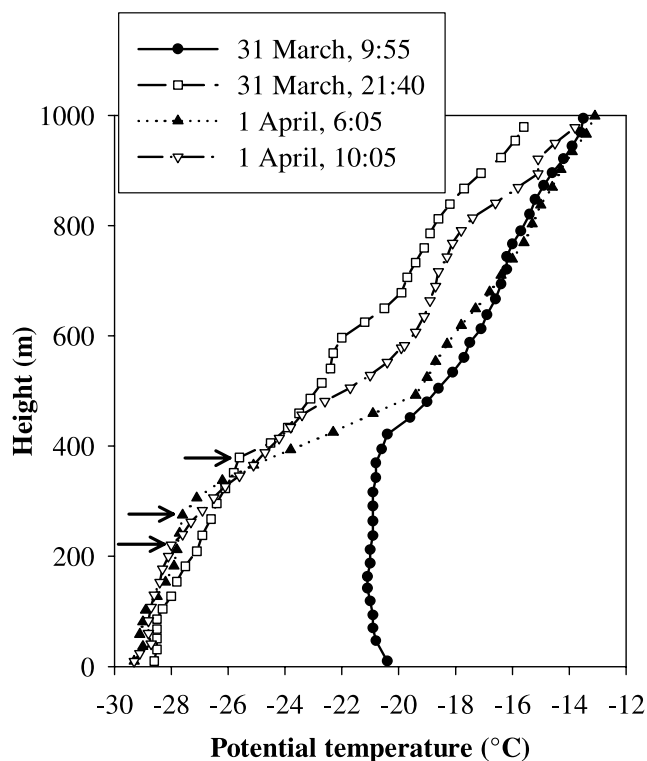
Figure 7. Profiles of the potential temperature measured on 31 March and 1 April. Arrows indicate the estimated heights of the boundary layer.
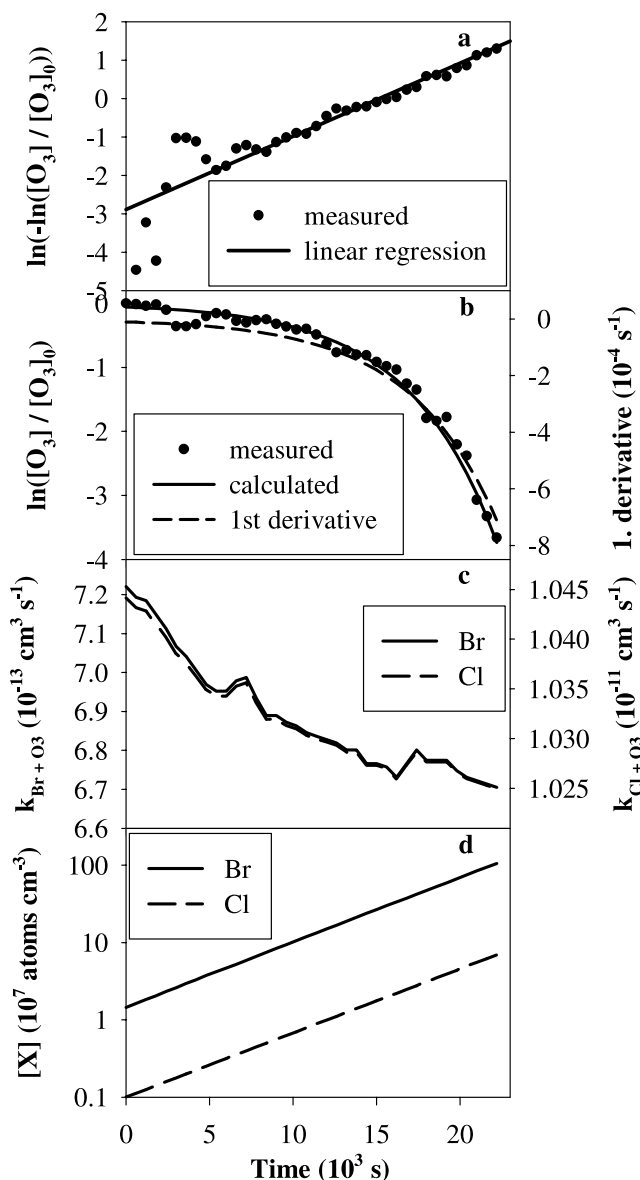
Figure 8. Analysis of the O_3 decay starting at 1130 UTC (31 March). (a) Plot of $\ln(-\ln([O_3]/[O_3]_0))$ versus time used to determine the coefficients a and b for equation (6); (b) logarithm of the relative O_3 concentrations versus time with the calculated fit according to equation (5) and calculated first derivative according to equation (7); (c) calculated temperature-dependent reaction rate coefficients for the reactions of Br and Cl with O_3; and (d) calculated halogen concentrations.

[21] The height of the boundary layer can be used to convert the BrO vertical column into mixing ratios. Assuming a mixing height of 380 m (Figure 7) and a BrO vertical column in the boundary layer of approximately $7 \cdot 10^{13}$ molecules cm^{-2} (Figure 6), a BrO concentration in the boundary layer of $1.8 \cdot 10^9$ molecules cm^{-3} results. This corresponds to a mixing ratio of 63 pptV in a well-mixed layer for the conditions on 31 March. These numbers are calculated assuming a uniform vertical BrO distribution in the boundary layer. However, the concentrations are possibly higher closer to the source of the reactive halogens. If this source was located at the surface it is likely hat a BrO concentration gradient was established with higher concentrations closer to the ground. Therefore the calculated BrO concentration has a rather high uncertainty on the order of approximately 50%. Nevertheless, The BrO mixing ratio was probably higher than the maximum values obtained from ground-based observations in the Arctic of ∼30 pptV [*Tuckermann et al.*, 1997; *Martinez et al.*, 1999; *Hönninger and Platt*, 2002]. As a consequence there is sufficient reactive bromine present locally in the boundary layer to explain the extremely fast O_3 depletion observed.

3.4. O_3 Measurements at Zeppelin Station

[22] Another indication that the ODE, observed along the track of the RV *Polarstern*, was a local phenomenon is given by a comparison with the O_3 mixing ratios measured at the Zeppelin Station. Relevant O_3 data obtained at this station show no evidence for a simultaneous ODE at Zeppelin Station (Figure 3). The backward trajectories indicate that the air masses reaching the station between 0500 and 1300 UTC on 1 April passed over the area, where the ODE was observed (Figure 1). Nevertheless, at Zeppelin Station the O_3 concentrations remained between levels of approximately 20 to 40 ppbV. A closer look at the trajectories reveals that the air masses sampled at Zeppelin station traveled at an elevation higher than 500 m, i.e., above the boundary layer in the region with depleted O_3. Thus the O_3 depletion was confined to the boundary layer whereas normal O_3 levels existed above the temperature inversion.

3.5. Kinetic Analysis of the O_3 Decay

[23] Being convinced that the observed ODE can be ascribed to chemical processes, the chemical kinetics of the observed decay can be analyzed. Figure 8 shows the logarithm of the O_3 concentration during the decay. A linear decrease would indicate a constant first-order loss. In contrast, Figure 8 demonstrates that the O_3 loss begins relatively slowly and accelerates during the decay period. This behavior is in excellent agreement with the so-called bromine explosion, which causes accelerating O_3 losses due to exponentially increasing reactive Br concentrations [*Wennberg*, 1999; *Platt and Hönninger*, 2003].

[24] Assuming that the catalytic destruction is dominated by reactions (R1) to (R4), a first-order loss of O_3 can be expected because of the Br reaction (R1). *Tuckermann et al.* [1997] pointed out that the self-reactions of BrO (R2 and R3) could be rate-limiting steps leading to either a zero-order or second-order O_3 loss depending on the O_3 concentration. However, for the conditions observed during this cruise, we assume an unlimited bromine source, leading to a continuous supply of Br_2, which is immediately photolyzed to Br (R4) as the actinic radiation intensities were sufficiently high in the afternoon of 31 March (Figure 4).

[25] Therefore the O_3 decay was analyzed assuming a first-order loss due to reaction (R1) resulting in the following rate law (1):

$$\frac{d[O_3]}{dt} = -k_{1st} \cdot [O_3] \tag{1}$$

$$[O_3] = [O_3]_0 \quad \exp(k_{1st} \quad t) \tag{2}$$

$$\ln \frac{[O_3]}{[O_3]_0} = k_{1st} \quad t \tag{3}$$

[26] $[O_3]_0$ is the O_3 concentration at the beginning of the decay (1130 UTC) determined from the measured mixing ratio of 39.7 ppbV. The first-order rate constant k_{1st} can be determined from the following equation:

$$\frac{d\left(\ln\left(\frac{[O_3]}{[O_3]_0}\right)\right)}{dt} = -k_{1st} \tag{4}$$

[27] The measured decrease of $\ln\left(\frac{[O_3]}{[O_3]_0}\right)$ versus time was fitted by a simple exponential equation:

$$\ln\left(\frac{[O_3]}{[O_3]_0}\right) = -\exp(b \cdot t + a) \tag{5}$$

$$\Leftrightarrow \ln\left(-\ln\left(\frac{[O_3]}{[O_3]_0}\right)\right) = b \cdot t + a \tag{6}$$

[28] The coefficients a and b are obtained from a linear regression of a plot of $\ln\left(-\ln\left(\frac{[O_3]}{[O_3]_0}\right)\right)$ versus time (Figure 8) resulting in values of a = $-(2.9 \pm 0.2)$ and b = $(1.9 \pm 0.1) \cdot 10^{-4}$ s^{-1} and a regression coefficient of $R^2 = 0.839$. Figure 8 shows the measured data together with the calculated curve according to equation (6) using the above mentioned values for a and b. The analytical solution of the first derivative of (6) finally gives the first-order rate constant k_{1st} of the observed O_3 decay as a function of time:

$$\frac{d\left(\ln\left(\frac{[O_3]}{[O_3]_0}\right)\right)}{dt} = -b \cdot \exp(b \cdot t + a) = -k_{1st} \tag{7}$$

[29] Assuming that the first-order decay is dominated by the reaction of O_3 with the halogens Br or Cl, we are able to calculate the concentrations needed as a function of time according to equation (9):

$$k_{1st} = k_{X+O3} \cdot [X] \tag{8}$$

$$[X] = \frac{k_{1st}}{k_{X+O3}} \tag{9}$$

[30] The rate constants k_{Br+O3} and k_{Cl+O3} for the reactions of Br and Cl with O_3 exhibit temperature dependencies according to the equations (10) and (11) [Sander et al., 2003].

$$k_{Br+O3} = 1.7 \cdot 10^{-11} \cdot \exp\left(-\frac{800}{T}\right) \tag{10}$$

$$k_{Cl+O3} = 2.3 \cdot 10^{-11} \cdot \exp\left(-\frac{200}{T}\right) \tag{11}$$

[31] The measured air temperature (Figure 4) was used to calculate rate constants for each measured O_3 concentration to derive the corresponding halogen concentration shown in Figure 8. Because of the different reactivities of O_3 toward the reactions with Br (slow) and Cl (fast), the halogen concentrations can serve as lower (Cl) and upper (Br) limits. The strong enhancement of the observed O_3 decay rates suggests that the halogen concentration also increase considerably. We find a good agreement if we assumed an exponential growth of the O_3 decay rate corresponding to an exponential increase of the halogen concentrations according to the so-called bromine explosion mechanism. If the Br reaction is solely responsible for the O_3 loss, the concentrations increase from $1.4 \cdot 10^7$ to almost $1.1 \cdot 10^9$ atoms cm^{-3} (corresponding to 37 pptV). On the other hand, the same loss can be caused by Cl concentrations increasing from $1 \cdot 10^6$ to $7 \cdot 10^7$ atoms cm^{-3}. However, these numbers necessarily exhibit large uncertainties for different reasons. The calculations only take into account the effect of the halogens separately as well as only the O_3 destruction by cycle 1. Therefore these values possibly represent only upper limits of the halogen concentrations. On the other hand, the numbers are calculated on the basis of the assumption that the halogens are homogenously distributed in the boundary layer. However, like in the case of BrO the possibility exists that a vertical gradient in the stable boundary layer can be established with higher concentrations closer to the source region, which might be the surface where the heterogeneous release of the halogens can take place. Taking this possibility into account the concentrations at the surface could be even higher than the calculated numbers. In summary, we estimate that the uncertainty of the calculated halogen concentrations is on the order of ±50%. Notwithstanding, the development of the halogen concentrations is consistent with the so-called bromine explosion mechanism.

[32] Even taking into account the large uncertainties the calculated halogen concentrations are surprisingly high. Previously reported halogen concentrations are based on the observation of the decay of different volatile organic compounds (VOC) [Jobson et al., 1994; Solberg et al., 1996; Ariya et al., 1998; Boudries and Bottenheim, 2000]. The halogen concentrations depend linearly on the periods, in which halogen chemistry was active. Assuming reaction times between 1 and 20 days the derived Cl and Br concentrations varied between 0.39 to $10 \cdot 10^4$ atoms cm^{-3} and 0.30 to $10 \cdot 10^7$ atoms cm^{-3}. In the case of Cl the numbers are significantly smaller than our calculated value of more than 10^6 atoms cm^{-3}, which is unrealistically high. On the other hand, the agreement for the Br concentrations is better although the upper limit of the Br concentration obtained here is still high compared to the literature values. However, the difference might be due to the fact that the VOC method delivers a spatial and temporal (daily) average, whereas we calculated here a Br concentration more representative for a shorter period and for a stable boundary layer. It seems possible that under these circumstances the Br concentrations can be higher than previously reported.

[33] Previous modeling studies [e.g., Fan and Jacob, 1992; Lehrer et al., 2004] clearly demonstrated that O_3 loss rates depend on the concentrations of reactive bromine compounds. While Lehrer et al. [2004] found that in the presence of 30 to 40 pptV of reactive bromine compounds the O_3 loss rate was in the order of 7.6 ppbV d^{-1}, Fan and Jacob [1992] calculated loss rates of approximately 40 ppbV d^{-1} in the presence of 100 pptV of reactive

bromine compounds. We observed an even higher average O_3 loss rate of 6.7 ppbV h^{-1} or 160 ppbV d^{-1} (Figure 3), which agrees well with the extremely high estimates of the Br mixing ratios with values of almost 40 pptV. Moreover, the observed rapid decay of O_3 is in agreement with the conclusions by *Hausmann and Platt* [1994]. On the basis of their measurements of BrO and O_3 in Alert, they argue that the O_3 depletion must be completed in less than one day to account for O_3 mixing ratios below 1 ppbV after the transport of the depleted air masses to the measuring site [*Hausmann and Platt*, 1994].

3.6. Influence of New Ice

[34] Having identified the ODE to be in the boundary layer and occurring close to the ship's position, other relevant and necessary conditions for the O_3 destruction were investigated. Figure 2 shows that the onset of the O_3 destruction occurred after the ship entered the MIZ, which was dominated by fields of new ice. The low air temperatures (Figure 4) measured in the MIZ make the formation of new sea ice very efficient. The trajectories (Figure 2) indicate that the air masses arriving at the ship during the O_3 decrease spent considerable time above the new ice fields in the MIZ suggesting that this is the region where the heterogeneous release of the reactive halogen compounds and the subsequent O_3 depletion took place. Unfortunately, areas with new sea ice are not characterized by a single sea salt containing surface, so that different types of surfaces can be considered for the heterogeneous release of the reactive halogens.

[35] For example, several investigations have demonstrated that temperatures below $-20°C$ coupled with open water areas are conditions favorable for the formation of frost flowers (FF) [*Perovich and Richter-Menge*, 1994; *Rankin et al.*, 2002]. Since both requirements were fulfilled in the MIZ, the surface conditions were optimal for the formation of FF. Accordingly, FF were recorded several times in the notes of the visual sea ice observations made during the cruise. Although there is some debate about the size of the specific surface areas of FF [*Rankin et al.*, 2002; *Domine et al.*, 2005], FF surfaces provide optimal conditions for the release of halogens because they are characterized by high salinities [*Rankin et al.*, 2002]. Presumably the Br^- and Cl^- in the FF is converted in the presence of HOBr to Br_2 and/or BrCl by heterogeneous reactions on or in the surface of the FF and subsequently released to the atmosphere: the source of HOBr being the gas phase reaction between HO_2 and BrO and subsequent migration to the surface. As a result, *Kaleschke et al.* [2004] found excellent spatial agreement between the occurrence of FF and enhanced BrO concentrations detected from GOME in both hemispheres.

[36] Nevertheless, FF are always accompanied by the formation of a liquid and highly saline layer on top of the sea ice [e.g., *Rankin et al.*, 2002]. This layer also offers ideal conditions for the heterogeneous reactions necessary for the halogen activation. Aerosols generated from FF can also be regarded as ideal surfaces for the heterogeneous reactions. In this case the source of the halogens would not be restricted to the sea ice surface, but could occur within the entire boundary layer if the aerosols are well distributed within this layer. Finally, *Simpson et al.* [2005] proposed

that sea-salt aerosols released from FF but deposited on the adjacent snowpack cold also contribute to the halogen activation. In that case the halogen release could occur over larger areas and not only over existing FF fields. Unfortunately, the current data set does not allow distinguishing between the roles of any of the described surfaces. Nevertheless, the conditions in the MIZ accompanied by the formation of new ice might be crucial parameters, which can possibly be used to estimate or model areas where the O_3 depletion in polar spring occurs.

[37] An alternative source of reactive bromine species is the photochemical conversion of halogenated organic or polyhalogenated compounds. These are produced in the Arctic Ocean by biological sources and subsequently released to the atmosphere [e.g., *Barrie et al.*, 1988; *Sturges et al.*, 1992] or stored under old sea ice. During this cruise, the biological activity was limited in the MIZ as indicated by the low concentrations of pelagic phytoplankton biomass and chlorophyll-a (J. N. Schwarz et al., manuscript in preparation, 2006). Both components showed higher concentrations farther south in the Fram Strait, where normal O_3 concentrations were observed. In summary, no evidence was found for the halogenated compounds being the source of the reactive bromine causing the observed ODE.

4. Conclusions

[38] Our observations show that during polar spring in the MIZ boundary layer O_3 can be completely removed within less than 7 hours. The observed removal was caused by local chemical processes as revealed by the analysis of air mass trajectories and further meteorological data. Simultaneously, a significant tropospheric column of BrO was retrieved from the measurements of SCIAMACHY. The efficient O_3 loss requires extremely high concentrations of reactive bromine, and is consistent with the BrO column retrieved from satellite data. Large fields of new ice characterized the MIZ during the observations. As a result of their properties and high bromide content, FF (or aerosols generated thereof either within the boundary layer or deposited on the snowpack) are well able to serve as the heterogeneous surface for the activation of such high levels of reactive bromine. However, contributions by reactions on other surfaces cannot be ruled out. Therefore further field studies in the MIZ and laboratory studies with FF are required to identify heterogeneous chemical processes occurring at the different kinds of surfaces. Nevertheless, the formation of new ice in combination with a stable atmospheric boundary layer possibly indicates a high probability of depleted surface O_3 concentrations. This has important implications for the determination of the extent of ODEs using remote sensing data.

References

Ariya, P. A., B. T. Jobson, R. Sander, H. Niki, G. W. Harris, J. F. Hopper, and K. G. Anlauf (1998), Measurements of C_2-C_7 hydrocarbons during

the Polar Sunrise Experiment 1994: Further evidence for halogen chemistry in the troposphere, *J. Geophys. Res.*, *103*(D11), 13,169–13,180.

Barrie, L. A., J. W. Bottenheim, R. C. Schnell, P. J. Crutzen, and R. A. Rasmussen (1988), Ozone destruction and photochemical reactions at polar sunrise in the lower Arctic atmosphere, *Nature*, *334*, 138–141.

Bottenheim, J. W., A. J. Gallant, and K. A. Brice (1986), Measurements of NO$_y$ species and O$_3$ at 82°N latitude, *Geophys. Res. Lett.*, *13*, 113–116.

Bottenheim, J. W., J. D. Fuentes, D. W. Tarasick, and K. G. Anlauf (2002), Ozone in the Arctic lower troposphere during winter and spring 2000 (ALERT2000), *Atmos. Environ.*, *36*(15/16), 2535–2544.

Boudries, H., and J. W. Bottenheim (2000), Cl and Br atom concentrations during a surface boundary layer ozone depletion event in the Canadian high Arctic, *Geophys. Res. Lett.*, *27*(4), 517–520.

Bovensmann, H., J. P. Burrows, M. Buchwitz, J. Frerick, S. Noël, V. V. Rozanov, K. V. Chance, and A. P. H. Goede (1999), SCIAMACHY—Mission objectives and measurement modes, *J. Atmos. Sci.*, *56*(2), 127–150.

Domine, F., A. S. Taillandier, W. R. Simpson, and K. Severin (2005), Specific surface area, density and microstructure of frost flowers, *Geophys. Res. Lett.*, *32*, L13502, doi:10.1029/2005GL023245.

Eppler, D., et al. (1992), Passive microwave signatures of sea ice, in *Microwave Remote Sensing of Sea Ice, Geophys. Monogr. Ser.*, vol. 68, edited by F. D. Carsey, pp. 47–71, AGU, Washington, D. C.

Fan, S.-M., and D. J. Jacob (1992), Surface ozone depletion in Arctic spring sustained by bromine reactions on aerosols, *Nature*, *359*, 522–524.

Hausmann, M., and U. Platt (1994), Spectroscopic measurement of bromine oxide and ozone in the high Arctic during Polar Sunrise Experiment 1992, *J. Geophys. Res.*, *99*, 25,399–25,414.

Hönninger, G., and U. Platt (2002), Observations of BrO and its vertical distribution during surface ozone depletion at Alert, *Atmos. Environ.*, *36*(15–16), 2481–2489.

Hopper, J. F., L. A. Barrie, A. Silis, W. Hart, A. J. Gallant, and H. Dryfhout (1998), Ozone and meteorology during the 1994 Polar Sunrise Experiment, *J. Geophys. Res.*, *103*(D1), 1481–1492.

Impey, G. A., P. B. Shepson, D. R. Hastie, L. A. Barrie, and K. G. Anlauf (1997), Measurements of photolyzable chlorine and bromine during the Polar Sunrise Experiment 1995, *J. Geophys. Res.*, *102*(D13), 16,005–16,010.

Jobson, B. T., H. Niki, Y. Yokouchi, J. Bottenheim, F. Hopper, and R. Leaitch (1994), Measurements of C$_2$-C$_6$ hydrocarbons during the Polar Sunrise 1992 Experiment: Evidence for Cl atom and Br atom chemistry, *J. Geophys. Res.*, *99*(D12), 25,355–25,368.

Kaleschke, L., C. Lüpkes, T. Vihma, J. Haarpaintner, A. Bochert, J. Hartmann, and G. Heygster (2001), SSM/I sea ice remote sensing for mesoscale ocean-atmosphere interaction analysis, *Can. J. Remote Sens.*, *27*(5), 526–537.

Kaleschke, L., et al. (2004), Frost flowers on sea ice as a source of sea salt and their influence on tropospheric halogen chemistry, *Geophys. Res. Lett.*, *31*, L16114, doi:10.1029/2004GL020655.

Lehrer, E., G. Hönninger, and U. Platt (2004), A one dimensional model study of the mechanism of halogen liberation and vertical transport in the polar troposphere, *Atmos. Chem. Phys.*, *4*, 2427–2440.

Martinez, M., T. Arnold, and D. Perner (1999), The role of bromine and chlorine chemistry for arctic ozone depletion events in Ny-Ålesund and comparison with model calculations, *Ann. Geophys.*, *17*(7), 941–956.

Oltmans, S. J., and W. D. Komhyr (1986), Surface ozone distributions and variations from 1973–1984 measurements at the NOAA Geophysical Monitoring for Climatic Change baseline observatories, *J. Geophys. Res.*, *91*(D4), 5229–5236.

Perovich, D. K., and J. A. Richter-Menge (1994), Surface characteristics of lead ice, *J. Geophys. Res.*, *99*(C8), 16,341–16,350.

Platt, U., and G. Hönninger (2003), The role of halogen species in the troposphere, *Chemosphere*, *52*, 325–338.

Rankin, A. M., E. W. Wolff, and S. Martin (2002), Frost flowers: Implications for tropospheric chemistry and ice core interpretation, *J. Geophys. Res.*, *107*(D23), 4683, doi:10.1029/2002JD002492.

Richter, A., F. Wittrock, M. Eisinger, and J. P. Burrows (1998), GOME observations of tropospheric BrO in Northern Hemispheric spring and summer 1997, *Geophys. Res. Lett.*, *25*, 2683–2686.

Ridley, B. A., et al. (2003), Ozone depletion events observed in the high latitude surface layer during the TOPSE aircraft program, *J. Geophys. Res.*, *108*(D4), 8356, doi:10.1029/2001JD001507.

Rozanov, A., H. Bovensmann, A. Bracher, S. Hrechanyy, V. Rozanov, M. Sinnhuber, F. Stroh, and J. P. Burrows (2005), NO$_2$ and BrO vertical profile retrieval from SCIAMACHY limb measurements: Sensitivity studies, *Adv. Space Res.*, *36*(5), 846–854.

Sander, S. P., et al. (2003), Chemical kinetics and photochemical data for use in atmospheric studies, evaluation 14, *JPL Publ. 02-25*, Jet Propul. Lab., Pasadena, Calif.

Schroeder, W. H., K. G. Anlauf, L. A. Barrie, J. Y. Lu, A. Steffen, D. R. Schneeberger, and T. Berg (1998), Arctic springtime depletion of mercury, *Nature*, *394*, 331–332.

Simpson, W. R., L. Alvarez-Aviles, T. A. Douglas, M. Sturm, and F. Domine (2005), Halogens in the coastal snow pack near Barrow, Alaska: Evidence for active bromine air-snow chemistry during springtime, *Geophys. Res. Lett.*, *32*, L04811, doi:10.1029/2004GL021748.

Solberg, S., N. Schmidbauer, A. Semb, F. Stordal, and Ø. Hov (1996), Boundary-layer ozone depletion as seen in the Norwegian Arctic in spring, *J. Atmos. Chem.*, *23*(3), 301–332.

Sturges, W. T., G. F. Cota, and P. T. Buckley (1992), Bromoform emission from Arctic ice algae, *Nature*, *358*, 660–662.

Tarasick, D. W., and J. W. Bottenheim (2002), Surface ozone depletion episodes in the Arctic and Antarctic from historical ozonesonde records, *Atmos. Chem. Phys.*, *2*(3), 197–205.

Tuckermann, M., R. Ackermann, C. Gölz, H. Lorenzen-Schmidt, T. Senne, J. Stutz, B. Trost, W. Unold, and U. Platt (1997), DOAS-observation of halogen radical-catalysed arctic boundary layer ozone destruction during the ARCTOC-campaigns 1995 and 1996 in Ny-Ålesund, Spitsbergen, *Tellus, Ser. B*, *49*(5), 533–555.

Vogt, R., P. J. Crutzen, and R. Sander (1996), A mechanism for halogen release from sea-salt aerosol in the remote marine boundary layer, *Nature*, *383*, 327–330.

Wagner, T., and U. Platt (1998), Satellite mapping of enhanced BrO concentrations in the troposphere, *Nature*, *395*, 486–490.

Wennberg, P. (1999), Bromine explosion, *Nature*, *397*, 299–301.

Wessel, S., S. Aoki, P. Winkler, R. Weller, A. Herber, H. Gernandt, and O. Schrems (1998), Tropospheric ozone depletion in polar regions—A comparison of observations in the Arctic and Antarctic, *Tellus, Ser. B*, *50*, 34–50.

Zeng, T., Y. Wang, K. Chance, E. V. Browell, B. A. Ridley, and E. L. Atlas (2003), Widespread persistent near-surface ozone depletion at northern high latitudes in spring, *Geophys. Res. Lett.*, *30*(24), 2298, doi:10.1029/2003GL018587.

————————

J. P. Burrows, A. Richter, and A. Rozanov, Institute of Environmental Physics, University of Bremen, P.O. Box 330440, D-28334 Bremen, Germany.

H.-W. Jacobi, Alfred Wegener Institute for Polar and Marine Research, Am Handelshafen 12, D-27570 Bremerhaven, Germany. (hwjacobi@awi-bremerhaven.de)

L. Kaleschke, Institute of Oceanography, Center for Marine and Atmospheric Research, University of Hamburg, D-20146 Hamburg, Germany.